Chin. Phys. Lett. **39**, 036801 (2022)

Structure and Wettability Engineering of Polycrystalline Diamond Films Treated by Thermally Oxidation, Second Growth and Surface Termination

Linfeng Wan(万琳丰)[1,2], Caoyuan Mu(牟草源)[1,2], Yaofeng Liu(刘尧峰)[1,2], Shaoheng Cheng(成绍恒)[1,2], Qiliang Wang(王启亮)[1,2*], Liuan Li(李柳暗)[1,2*], Hongdong Li(李红东)[1,2*], and Guangtian Zou(邹广田)[1,2]

[1]*State Key Lab of Superhard Materials, College of Physics, Jilin University, Changchun 130012, China*
[2]*Shenzhen Research Institute, Jilin University, Shenzhen 518057, China*

(Received 2 November 2021; accepted 30 December 2021; published online 1 March 2022)

High-quality polycrystalline diamond films with dominated (100)-oriented grains are realized by combining the thermally oxidation and the homogeneous second growth processes. Moreover, we investigate the wettability property of the polycrystalline diamonds in various stages. Different surface structures (with various grain sizes, voids, and orientations, etc.) and terminations (hydrogen or oxygen) have significant effects on the wettability of polycrystalline diamond films. The wettability is further closely related to the polarity of solutions. By measuring the contact angle and calculating the dispersion and polarity components, we estimate the surface energy of polycrystalline diamond films, and explore the factors affecting the surface energy. The modulations in growth quality and wettability property of polycrystalline diamond films provide valuable data for development of diamond-based multiple devices in practical applications.

DOI: 10.1088/0256-307X/39/3/036801

Diamond, as an allotrope of carbon, is a promising material for electrochemical and bio-sensing applications (especially in harsh environment) because of its wide band-gap, chemical stability and biocompatibility.[1,2] In the past years, diamond ion-sensitive field-effect transistors have been demonstrated for pH sensor applications.[3] Furthermore, the sensitivity and chemical stability of the devices present an obvious dependency on the surface termination. In addition, the diamond meshes showing highly efficient water–oil separation and water droplet transference are realized by adjusting the surface termination.[4] Usually, the wettability of diamond can be adjusted into hydrophobic or hydrophilic through hydrogen (H) and oxygen (O) terminations, respectively.[4–6] Until now, many kinds of methods have been developed to modify the surface termination such as the *in situ* oxygen/water vapor etching, thermal oxidation in oxygen, acid and alkali treatments, as well as the electrochemical oxidation.[4–9]

On the other hand, although those devices with high performances can be designed and fabricated on both single crystal diamond (SCD) and polycrystalline diamond (PCD) substrates, the chemical vapor deposition (CVD) PCD films grown on heterogeneous substrates are more preferable due to the low cost. However, the PCD films normally consist of numerous grains with various orientations and abundant boundaries. The high density non-diamond carbon phases appearing at grain boundaries will degrade the device performance and long-term reliability, especially when they work in aggressive acid or alkali solutions and high bias condition. Therefore, it is necessary to control and reduce the grain boundary density, which helps to suppress the non-diamond phase defects. Heteroepitaxial diamond films on iridium (Ir) coated substrates are generally proved to be an effective route, which helps to decrease the dislocation density from 10^{10} to $10^{8}\,\mathrm{cm}^{-2}$.[10] However, Ir is expensive and additional complex oxide buffer layers are highly desirable.

We previously confirmed that the thermal oxidation under proper conditions eliminates selectively nano-diamonds and non-diamond carbons in the films.[11] Here, high-quality PCD films with dominated (100) grains are achieved by a thermally oxidizing treatment and following a second growth process. It is demonstrated that the etching of non-diamond phase during thermally oxidation effectively improves the quality of the second growth layer. Then, the relationship between surface hydrogen (H)- or oxygen (O)-termination and wettability is also analyzed. The surface energy of the samples are calculated for the corresponding structures and surface terminations.

The PCD films with (100) surface were deposited on molybdenum substrate in an area of $1 \times 1\,\mathrm{cm}^2$ by 5 kW microwave plasma CVD (MPCVD) system at 2.45 GHz. The reactor pressure varied in the range from 80 torr to 120 torr, the substrate temperature was monitored at around 1000 ℃ by the optical py-

*Corresponding authors. Email: wangqiliang@jlu.edu.cn; liliuan@jlu.edu.cn; hdli@jlu.edu.cn
© 2022 Chinese Physical Society and IOP Publishing Ltd

rometer. The $H_2/CH_4/N_2$ flow rates into the chamber were set to 200/2/2 sccm, respectively. The addition of gaseous N_2 could enhance the highly (100)-textured films growth.[12,13] After deposition for 20 h with a microwave power of 2000 W, a 140-μm-thick film (measured by a microcalliper) was peeled off from the substrate during the cooling process, due to the large discrepancy in thermal expansion coefficient between diamond and molybdenum. The as-grown free-standing diamond film (named as sample A) was cut into pieces with dimensions of $5 \times 5\,\text{mm}^2$. The as-prepared diamond films were thermally treated at 800 ℃ for 15 min in air. The majority of nanocrystalline diamond and/or nondiamond-phase carbonaceous nanoparticles appearing at grain boundaries could be oxidized and vaporized, and the large micro-sized grains were maintained.[5,11] This treated sample was named as sample B. The oxidized sample was sent back to the MPCVD chamber for the second growth process (sample C). The growth condition was similar to sample A without introducing nitrogen, which could reduce the quality degradation caused by nitrogen doping.

The surface morphology, structure and crystal orientation were characterized by means of scanning electron microscopy (SEM, FEIMAGELLAN-400), and x-ray diffraction instrument (XRD, Rigaku D/MAX 2550 V/PC). The contact angles (θ) were measured by a liquid droplet shape analysis system (XE-CAMC33). The volume of liquid droplet was about 0.5 μL. The Owen–Wendt–Rabel–Kaelble method[14] was used to calculate the surface energy. In order to study the wettability and surface energy of both H- and O-terminated surfaces of PCD films, the samples were further hydrogenated (sample B with original O-termination) and oxidized (samples A and C with original H-termination). Hydrogenated treatment was realized by exposing in H plasma (the treatment conditions were as follows: the reaction gas was H_2 with 200 sccm, microwave power was 2000 W, chamber pressure was 80 torr, and substrate temperature was 800 ℃). The oxygenated treatment was realized by heat treatment in air at 400 ℃ for 30 min.

Figure 1(a) presents the surface SEM morphology of the as-grown PCD films. The surface is dominated by squared grains with an obvious (100)-oriented face and an average side length of approximately 30 μm. The spiral growth terraces are observed on the surface of part of the crystal grains. Those terraces are related to the screw-dislocation-induced spiral growth mode.[15] In addition, the crystalline quality of the regions between (100) grains is inferior with many terraces, where a lot of nano-diamonds and non-diamond phase exist.[11,16,17] After high temperature oxidation treatment [Fig. 1(b)], the terraces around the (100) grains are selectively removed. It was reported that the (100) plane of diamond presented better thermal stability in oxygen than other planes.[11,18,19] Therefore, some tiny non-(100) oriented diamond and non-diamond phases among the large grains were easily oxidized into carbon dioxide during high temperature treatment in air, resulting in the remains of micron-sized columnar (100) diamond grains.[11] The possible mechanism is that the defect structure of the nanocrystalline grains, non-diamond phase, as well as the dislocations, possess high density of dangling bonds, which are easier to chemically react with oxygen than those large (100) diamond grains. For the re-grown sample [Fig. 1(c)], the lateral growth and coalescence of residual (100) diamond grains are enhanced, resulting in a flatten surface and a lower density of grain boundaries. Furthermore, in comparison with the surface morphology of the as-grown PCD film [Fig. 1(a)], the nano-diamond particles are greatly reduced, and the quality of the re-grown sample is significantly improved.

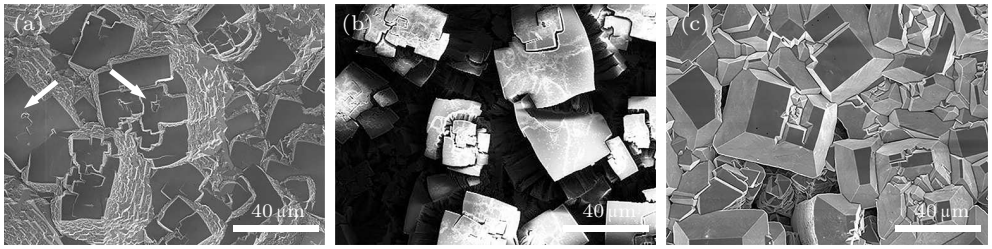

Fig. 1. The SEM surface morphology of the (a) as-grown PCD film, (b) PCD film after thermally treatment in air, and (c) re-grown PCD film. The arrows in (a) indicate the screw-dislocation-related growth terraces.

Figure 2 shows the cross-sectional SEM images of the samples cleaved along the growth direction corresponding to Fig. 1. We can see that from Fig. 2(a) a typical V-shape column growth from the nucleation layer to surface at the first growth process, namely, the crystal grains grow in longitudinal and lateral directions simultaneously with the increase of deposition time. Then, high densities of nanocrystalline grains, as well as non-diamond phase (marked in the yellow rectangle), are generated within grain boundaries until the coalescence of (100) grains, which leads to degradation of the crystalline quality of the PCD films. Figure 2(b) shows the cross-sectional morphology of the sample after high-temperature oxidation treatment, in which the terraces around the (100) crystalline grains are selectively removed, and large-size (100) diamond

grains remain with a V-shape. With the re-growing of PCD film, it is shown in Fig. 3(c) that the main (100) diamond grains having lateral growth becomes larger and flatter.

The as-grown diamond film was deposited on a molybdenum substrate firstly, which is a typical heteroepitaxial nucleation growth. A large number of nano-diamond particles and non-diamond phase carbon appeared during the growth process, resulting in poor crystalline quality. After high-temperature annealing treatment in air, the nano-diamond and non-diamond phase carbon at the grain boundaries of the high quality large-sized grains can be effectively removed. The following secondary growth mainly occurs on those remained diamond grains, which can be seen as a homoepitaxial growth mode. As a result, the homoepitaxial growth leads to significant improvement on quality of the second-grown layer.

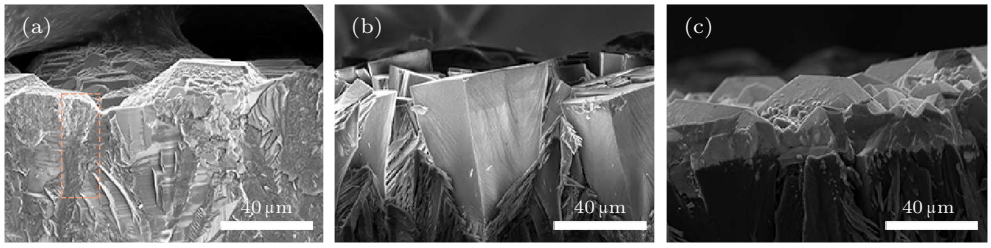

Fig. 2. The cross-sectional SEM morphology of the (a) as-grown PCD film, (b) PCD film after thermally treatment in air, and (c) re-grown PCD film.

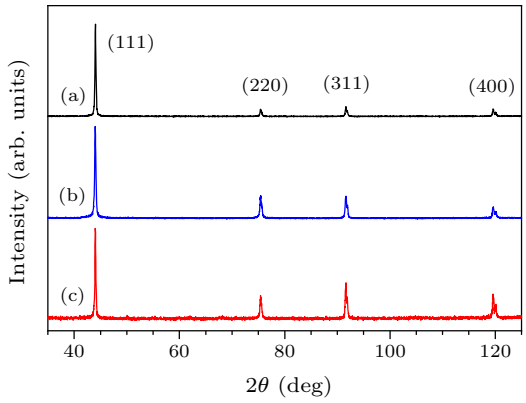

Fig. 3. XRD spectra of PCD films in different stages: (a) as-grown, (b) after thermal treatment, and (c) re-grown. The spectra are normalized by the (111) peak.

Figure 3 shows the XRD spectra of the PCD films in the three stages, i.e., as-growth, thermal treatment in air, and re-growth. All the samples show four diffraction peaks at 44.0°, 75.4°, 91.7°, and 119.7°, corresponding to diamond (111), (220), (311), and (400) crystal planes, respectively. The integrated intensity ratio of the (111) and (400) planes ($I_{(111)}/I_{(400)}$) is used to evaluate the variation of crystalline structure and orientation for different samples. It is found that the (111) peak dominates the XRD spectrum of the as-grown PCD films with an $I_{(111)}/I_{(400)}$ of approximately 11.5. On the one hand, the x-ray diffraction factor is much higher for the (111) plane, compared to that of the (400) plane.[20] On the other hand, there are abundant (111) grains between (100) grains. For the sample after high temperature oxidation treatment, the (111) diffraction peak intensity is decreased with an $I_{(111)}/I_{(400)}$ of approximately 7.4 due to the selective etching. Finally, the re-grown process further decreases the $I_{(111)}/I_{(400)}$ to approximately 3.4, which could be ascribed to the lateral growth and coalescence of residual (100) diamond grains. Note that the spectrum is still dominated by the (111) peak since the additional re-grown (100) diamond layer is thinner compared with the total thickness, as shown in the SEM morphology.

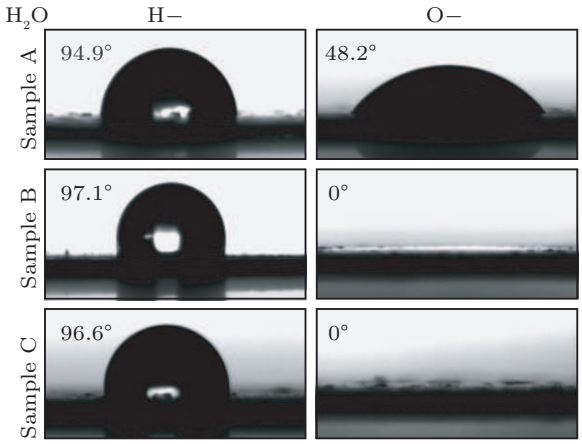

Fig. 4. Contact angle images of water droplets on sample A (as-grown), sample B (thermally treated), and sample C (re-grown) of diamond films with H- and O-terminations.

We choose polar deionized water (H_2O) and non-polar di-iodomethane (CH_2I_2) as the test solution for the wettability examinations of those samples. The wettability features of the three samples with different terminations for deionized H_2O (polar liquid) and CH_2I_2 (non-polar liquid) are presented in Figs. 4 and 5, respectively. The corresponding contact angles are summarized in Table 1.

With a droplet of deionized H_2O, the three samples with H-terminated surface present a contact angle larger than 90°, indicating a hydrophobic property for the polar liquid. After the surface termination is changed into oxygen, the contact angles decrease to ∼48.2° (hydrophilic), ∼0° (super-hydrophilic), and

∼0° (super-hydrophilic) for samples A, B, and C, respectively. However, the contact with non-polar CH_2I_2 shows an obviously different behavior. The H-terminated and O-terminated surfaces of all samples are hydrophilic, showing the relatively obvious difference in contact angles. Sample A shows ordinary hydrophilicity for both terminations, implying that hydrogen/oxygen termination has less influence on the wettability. After high-temperature oxidation treatment, sample B has contact angles of ∼0° and ∼6.8° (super-hydrophilic) on the H-terminated and O-terminated surfaces, respectively, which is attributed to the additional voids appearing on the thermally treated surface of PCD films. Sample C shows the super-hydrophilic property on the H-terminated surface, and ordinary hydrophilic behavior on the O-terminated surface. As for the cases of H_2O droplet on O-termination of samples B and C (Fig. 4) and CH_2I_2 droplet on H-termination of samples B and C (Fig. 5), the contact angles are nearly 0°. On the one hand, the surfaces of those samples are super-hydrophilic, and on the other hand, the rough and porous surface could drag the H_2O or CH_2I_2 droplets beneath the porous top surface of the films.

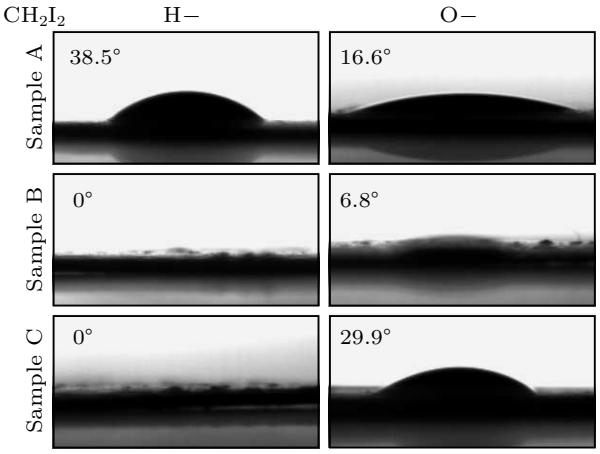

Fig. 5. Contact angle images of di-iodomethane droplets on sample A (as-grown), sample B (thermally treated), and sample C (re-grown) of diamond films with H- and O-terminations.

Table 1. The average contact angles of sample A (as-grown), sample B (thermally treated), and sample C (re-grown) of diamond films with H- and O-terminations.

Samples	Termination	H_2O	CH_2I_2
Sample A	–H	94.9° ± 1.1°	38.5° ± 1.2°
	–O	48.2° ± 0.4°	16.6° ± 0.5°
Sample B	–H	97.1° ± 2.4°	∼0°
	–O	∼0°	6.8° ± 0.5°
Sample C	–H	96.6° ± 0.6°	∼0°
	–O	∼0°	29.9° ± 0.9°

Surface energies $\gamma_{S/L}$ (γ_S for solid and γ_L for liquid) are important parameters determining surface properties of materials, which is composed of the polarity and dispersion components as expressed by the equation[21]

$$\gamma_{S/L} = \gamma^P_{S/L} + \gamma^D_{S/L}, \tag{1}$$

where $\gamma^P_{S/L}$ and $\gamma^D_{S/L}$ are the polarity and dispersion contributions, respectively. To measure the free energy of solid surface under ambient conditions, an indirect method starts with Young equation[22]

$$\gamma_S = \gamma_{SL} + \gamma_L \cos\theta \tag{2}$$

for liquid, solid and vapor in equilibrium with a force balance, where γ_S is the solid surface/vapor energy (tension), γ_{SL} is the solid-liquid interfacial energy, γ_L is the vapor/liquid tension, and θ is the contact angle between a liquid drop and the solid surface. For the force balance, it can be considered as an energy balance because an interfacial tension of force per unit length is equivalent to an energy per unit area.[23]

In this study, the surface energy of diamond films is calculated by the Owen–Wendt–Rabel–Kaelble equation:[14]

$$\gamma_{SL} = \gamma_S + \gamma_L - 2\sqrt{\gamma^D_S \cdot \gamma^D_L} - 2\sqrt{\gamma^P_S \cdot \gamma^P_L}, \tag{3}$$

where γ^D_S (γ^D_L) is the dispersion energy of solid (liquid), γ^P_S (γ^P_L) is polarity energy of solid (liquid).

Table 2. Surface energy γ_S, dispersion γ^D_S, and polarity γ^P_S components of sample A (as-grown), sample B (thermally treated), and sample C (re-grown) of diamond films with H- and O-terminations.

	Termination	γ^D_S (mJ/m^2)	γ^P_S (mJ/m^2)	γ_S (mJ/m^2)
Sample A	–H	40.9	0.2	41.1
	–O	38.1	19.9	58.0
Sample B	–H	54.3	0.1	54.4
	–O	34.7	40.2	74.9
Sample C	–H	54.1	0.1	54.2
	–O	28.6	44.8	73.4

The surface energies of polar deionized H_2O (non-polar CH_2I_2) used in the calculation are as follows:[24] the surface energy γ_L is 72.8 mJ/m^2 (50.8 mJ/m^2), the dispersion γ^D_L is 21.8 mJ/m^2 (50.8 mJ/m^2), and the polarity γ^P_L is 51.0 mJ/m^2 (0 mJ/m^2) for deionized H_2O (CH_2I_2). Based on the measured contact angle data and Eqs. (1)–(3), the calculated surface energy γ_S, dispersion γ^D_S, polarity γ^P_S are obtained and summarized in Table 2.

In general, polarity component represents the degree of charge deviation of molecules. The enlarged charge deviation and electric dipole moment lead to the increase of polarity. Because oxygen-terminated diamond has enhanced polarity, it has a strong adsorption effect on polar molecules.[5] The wettability feature with a modulated surface polarity could be applied widely in the fields of catalyst, optoelectronics, etc.[25] As presented in Table 2, the proportion of the polarity component on the O-terminated diamond surface is much higher than that of the H-terminated diamond surface. Generally, the discrepancy of electron affinity between C and O is higher than that of C

and H.[26] Then, the C–O bond on the O-terminated diamond surface exhibits greater polarity than the C–H bond. The dipole on the surface helps to attract the H_2O molecule and to decrease the contact angle. Therefore, for polar deionized H_2O, the H-terminated surface with a small polarity component presents a contact angle larger than 90°. It is worth noting that the highest contact angle of polar H_2O is recorded for the sample A with O-termination, even it presents a smaller polarity component, which can be ascribed to the high density of non-diamond defects. The defects are easy to bond with H atoms and hinder the formation of O-termination. After thermal oxidation (for sample B) and subsequent second-growth process (for sample C), the increases of voids and roughness appear with O-termination enhanced polarity component, and consequently, the contact angles become zero for both samples.

For the non-polar di-iodomethane (CH_2I_2), theoretically, the contact angle has no direct relationship with the polarity component and would be mainly determined by the dispersion. Combining Tables 1 and 2, a relatively larger dispersion tends to generate a smaller contact angle. However, the sample B having O-termination with a medium dispersion shows a smallest contact angle, which can be caused by the void-filling effect of the solution on the film. Sample C with O-termination presents the smallest dispersion and the largest contact angle. The possible reason is that the bonding status on the high quality (100) plane is uniform and stable, resulting in the slight variation. In fact, there are many kinds of factors such as crystal orientation, surface termination, surface structure, grain size, and roughness, which affect the wettability and surface energy.[5] Therefore, the data recorded in this work provide additional information of diamond features and properties in various stages.

In summary, we have reported a second-growth process for improving quality of chemical vapor deposited PCD films, and the wettability property is demonstrated to be related to its surface structure and termination. An as-grown PCD film with (100)-oriented surface is thermally oxidized in air for removing the randomly orientated micro-polycrystalline grains around the boundaries, and a homogeneous second-growth process is followed. The secondly grown layer consists of enlarged grains with high (100) orientation and smooth surface. For the PCD samples, terminations of oxygen and hydrogen are performed to investigate the behavior of wettability and related physical parameters. In addition, the wettability and surface energy of diamond in different stages show obvious differences, and the wettability is related to the surface energy with dispersion and polarity components of diamond, which are determined by surface roughness and surface termination. This work provides a method of thermal oxygen-etching and second growth to improve the quality of PCD films and modulate the surface wettability, which are favorable for constructing high performance diamond-based multifunctional devices.

Acknowledgements. This work was supported by the Key-Area Research and Development Program of Guangdong Province (Grant No. 2020B0101690001), and the National Natural Science Foundation of China (Grant No. 51972135).

References

[1] Sussmann R S 2009 *CVD Diamond for Electronic Devices and Sensors* (New York: Wiley)
[2] Umezawa H 2018 *Mater. Sci. Semicond. Process.* **78** 147
[3] Dipalo M, Gao Z, Scharpf J *et al.* 2009 *Diamond Relat. Mater.* **18** 884
[4] Yang Y Z, Li H D, Cheng S H, Zou G T, Wang C X and Lin Q 2014 *Chem. Commun.* **50** 2900
[5] Ma Z C, Gao N, Cheng S H, Liu J S, Yang M C, Wang P, Feng Z Y, Wang Q L and Li H D 2020 *Chin. Phys. Lett.* **37** 046801
[6] Ostrovskaya L, Perevertailo V, Ralchenko V, Dementjev A and Loginova O 2002 *Diamond Relat. Mater.* **11** 845
[7] Gribanova E V, Zhukov A N, Antonyuk I E, Benndorf C and Baskova E N 2000 *Diamond Relat. Mater.* **9** 1
[8] Klauser F, Ghodbane S, Boukherroub R, Szunerits S, Steinmüller-Nethl D, Bertel E and Memmel N 2010 *Diamond Relat. Mater.* **19** 474
[9] Zhang X F, Cui Y X, Liu X B, Sui T Y, Ji C H and Zhang D W 2019 *Surf. Coat. Technol.* **375** 681
[10] Stehl C, Fischer M, Gsell S, Berdermann E, Rahman M S, Traeger M, Klein O and Schreck M 2013 *Appl. Phys. Lett.* **103** 151905
[11] Pei X Q, Cheng S H, Ma Y B, Wu D F, Liu J S, Wang Q L, Yang Y Z and Li H D 2015 *Appl. Surf. Sci.* **346** 189
[12] Asmussen J, Mossbrucker J, Khatami S, Huang W S, Wright B and Ayres V 1999 *Diamond Relat. Mater.* **8** 220
[13] Li H D, Zou G T, Wang Q L, Cheng S H, Li B, Lü J N, Lü X Y and Jin Z S 2008 *Chin. Phys. Lett.* **25** 1803
[14] Owens D and Wendt R C 1969 *J. Appl. Polym. Sci.* **13** 1741
[15] Tokuda N, Ogura M, Matsumoto T, Yamasaki S and Inokuma T 2016 *Phys. Status Solidi A* **213** 2501
[16] Luo K, Liu B, Sun L, Zhao Z and Tian Y J 2021 *Chin. Phys. Lett.* **38** 028102
[17] Lv R Y, Yang X G, Yang D W *et al.* 2021 *Chin. Phys. Lett.* **38** 076101
[18] Obraztsov A N, Kopylov P G, Chuvilin A L and Savenko N V 2009 *Diamond Relat. Mater.* **18** 1289
[19] Zolotukhin A A, Dolganov M A, Alekseev A M and Obraztsov A N 2014 *Diamond Relat. Mater.* **42** 15
[20] Pecharesky V K and Zavalij P Y 2005 *Fundamentals of Powder Diffraction and Structural Characterization of Materials* (New York: Springer)
[21] Fowkes F 1968 *Chemistry and Physics of Interfaces* (Washington, DC: American Chemical Society Publications)
[22] Young T 1805 *Philos. Trans. R. Soc.* **95** 65
[23] Adamson W and Gast A P 1997 *Physical Chemistry of Surfaces* (New York: Wiley Publishing)
[24] Pinzari F, Ascarelli P, Cappelli E, Mattei G and Giorgi R 2001 *Diamond Relat. Mater.* **10** 781
[25] Cui J B, Graupner R, Ristein J and Ley L 1999 *Diamond Relat. Mater.* **8** 748
[26] Weide J V D, Zhang Z, Baumann P K, Wensell M G, Bernholc J and Nemanich R J 1994 *Phys. Rev. B* **50** 5803